NMR Studies Reveal an Unexpected Binding Site for a Redox Inhibitor of AP Endonuclease 1

ARTICLE *in* BIOCHEMISTRY · DECEMBER 2011

Impact Factor: 3.02 · DOI: 10.1021/bi201071g · Source: PubMed

4 AUTHORS:

Brittney Manvilla
University of Chicago
9 PUBLICATIONS **63** CITATIONS
SEE PROFILE

Orrette R Wauchope
Vanderbilt University
12 PUBLICATIONS **95** CITATIONS
SEE PROFILE

Katherine L Seley-Radtke
University of Maryland, Baltimore County
83 PUBLICATIONS **681** CITATIONS
SEE PROFILE

Alexander C Drohat
University of Maryland, Baltimore
48 PUBLICATIONS **1,900** CITATIONS
SEE PROFILE

Published in final edited form as:
Biochemistry. 2011 December 6; 50(48): 10540–10549. doi:10.1021/bi201071g.

NMR Studies Reveal an Unexpected Binding Site for a Redox Inhibitor of AP Endonuclease 1

Brittney A. Manvilla[‡], **Orrette Wauchope**[£], **Katherine L. Seley-Radtke**[£], and **Alexander C. Drohat**[*,‡,§]

[‡]Department of Biochemistry and Molecular Biology, University of Maryland School of Medicine, Baltimore, MD 21201, United States

[§]Greenebaum Cancer Center, University of Maryland School of Medicine, Baltimore, MD 21201, United States

[£]Department of Chemistry and Biochemistry, University of Maryland Baltimore County, Baltimore, MD 21250, United States

Abstract

AP endonuclease 1 (APE1) is a multi-faceted protein with essential roles in DNA repair and transcriptional regulation. APE1 (Ref-1) activates many transcription factors (TF), including AP-1 and NF-κB. While the mechanism of APE1 redox activity remains unknown, it may involve reduction of an oxidized Cys in the TF DNA-binding domain. Several small molecules inhibit APE1-mediated TF activation, including the quinone derivative E3330. It has been proposed some inhibitors bind near C65, a residue suggested to be important for TF activation, but the binding site has not been determined for any inhibitor. Remarkably, NMR and molecular docking studies here reveal E3330 binds in the DNA repair active site of APE1, far removed from C65. Accordingly, AP endonuclease activity is substantially inhibited by E3330 (100 μM), suggesting that E3330 may not selectively inhibit APE1 redox activity in cells, in contrast with previous proposals. A naphthoquinone analog of E3330, RN7-60, binds a site removed from both C65 and the repair active-site. While a detailed understanding of how these inhibitors work requires further studies into the mechanism of redox activity, our results do not support proposals that E3330 binds selectively (and slowly) to locally unfolded APE1, or that E3330 promotes formation of disulfide bonds in APE1. Rather, we suggest E3330 may suppress a conformational change needed for redox activity, disrupt productive APE1-TF binding, or block the proposed redox chaperone activity of APE1. Our results provide the first structural information for any APE1 redox inhibitor, and could facilitate development of improved inhibitors for research and perhaps clinical purposes.

AP endonuclease 1 (APE1) is a multi-functional protein with essential roles in DNA repair and transcriptional regulation. APE1 is required for repair of apurinic/apyrimidinic (AP) sites and other mutagenic and cytotoxic DNA lesions, and is a central element of base excision repair and DNA strand break repair pathways (1–3). In one of its regulatory roles, APE1 serves as a *trans*-acting factor as part of a protein complex that binds negative Ca^{2+}-response elements (nCaRE) to down-regulate genes such as PTH and renin, a function promoted by p300-mediated acetylation of APE1 (4, 5). This regulatory role and the DNA repair functions of APE1 are essential for embryonic development and cell viability (6–8).

[*]Corresponding author. adrohat@som.umaryland.edu, Phone (410) 706-8118, Fax (410) 706-8297.

SUPPORTING INFORMATION AVAILABLE

The supporting information contains additional NMR spectra for APE1 and APE1 ^{N38}-W280A, and dynamic light scattering data for APE1 and APE1 ^{N38}. This material is available free of charge via the Internet at http://pubs.acs.org.

In a distinct regulatory function, APE1 was found to activate the transcription factor AP-1 (c-Jun/c-Fos) via a redox (reduction-oxidation) mechanism, thus APE1 is also known as Ref-1 (redox effector factor 1) (9, 10). APE1 activates AP-1 by mediating the reduction of a Cys residue in its DNA binding domain, and APE1 was subsequently shown to activate many other transcription factors in a similar manner, including NF-κB, HIF-1α, p53, and RARα, among others (5, 10).

While the catalytic residues and active site for the DNA repair activity of APE1 are established, the same cannot be said for its redox activity. Much attention has focused on the seven conserved Cys residues in mammalian APE1, and an initial study with recombinant APE1 and Cys→Ala mutants concluded that C65 (human APE1) is essential for redox activity *in vitro* (11). However, crystal structures of APE1, free and DNA-bound, show that C65 is buried, indicating a major conformational change would be required for C65 to mediate the reductive activation of transcription factors (12, 13). A subsequent study found that mice homozygous for the C64A variant of APE1 (equivalent to C65 in human APE1) survive to normal life expectancy with no overt abnormal phenotype, that cell extracts from these mice exhibit normal AP-1 DNA binding activity, and that recombinant C64A mouse APE1 has normal AP-1 reducing activity (in cell extracts), altogether indicating C64 (C65 human) is not essential for redox activity (14). A recent study shows APE1 can enhance the activation of transcription factors provided by GSH or thioredoxin (Trx), and this function is retained for APE1 that lacks all Cys residues (Cys→Ser), indicating a “redox chaperone” mechanism for APE1 activation of transcription factors (15). Nevertheless, the potential role of C65 remains controversial, and more recent studies conclude C65 is important for redox activity (16, 17), including a report that redox-inactive zebrafish APE1 gains redox activity upon Thr→Cys mutation at the site equivalent to C65 of human APE1.

Despite ambiguity regarding the mechanism of APE1 redox activity, numerous compounds have been reported to inhibit APE1 redox activity *in vitro* and *in vivo*. The most well studied example is a quinone derivative known as E3330 or (*E*)-3-(5, 6-dimethoxy-3-methyl-14-dioxocyclohexa-25-dienyl)-nonylpropenoic acid, the first inhibitor of APE1 redox activity to be discovered (18–20). Previous studies indicate E3330 binds specifically to APE1, and it has been proposed that E3330 selectively inhibits its redox but not its DNA repair activity (16, 17, 19). Recent studies have identified many new compounds that inhibit APE1 redox activity, some more effectively than E3330 (21, 22). Efforts to develop inhibitors of APE1 redox activity are driven in part by findings that such compounds could potentially lead to drugs that are useful for treating diseases including cancer (22–25). Such inhibitors are potentially important research tools for elucidating the effects of selectively inhibiting APE1 redox activity, which cannot be accomplished by suppressing APE1 levels given its essential roles in DNA repair and as a trans-acting transcriptional cofactor (17, 26).

While the development of novel redox inhibitors would benefit from structural information regarding APE1-inhibitor interactions, no structural data is available to date for any redox (or repair) inhibitor. Given that some studies implicate C65 in redox activity, it has been inferred that redox inhibitors bind near C65 (17), but the binding site remains unknown for any inhibitor. To address this issue, we used NMR chemical shift perturbation experiments and molecular docking studies to elucidate the binding site for E3330. Such an approach is enabled by our recent determination of the chemical shift assignments for APE1 (27). In addition, we synthesized another APE1 redox inhibitor, (*E*)-3-(3-chloro-1,4-naphthoquinon-2-yl)-2-methylpropenoic acid, also known as RN7-60, which is reported to inhibit redox activity more efficiently than E3330 (21, 22), and we determined the binding site for RN7-60. Using the NMR data, we also determined the dissociation constant (K_d) for E3330 and RN7-60. Additionally we reassessed the effect of E3330 on both APE1 repair and redox activity. Our results have implications for previously suggested mechanisms by

which these compounds inhibit APE1 redox activity, and provide new structural information that could facilitate the development of improved redox inhibitors which may have important research and clinical applications.

MATERIALS AND METHODS

Materials

Full length APE1 and a construct lacking the 38 N-terminal residues ($APE1^{\Delta N38}$) were expressed in *E coli* and purified (at 4 °C) as previously described (27, 28), including Ni-affinity chromatography (Qiagen), overnight thrombin cleavage of the N-terminal poly-His tag, and ion exchange chromatography using a 5 ml HiTrap SP HP column (GE Healthcare). The resulting APE1 and $APE1^{\Delta N38}$ was >99 % pure as judged by SDS-PAGE (coomassie stained gel). The concentration of both constructs was determined by absorbance using a molar absorption coefficient of $\varepsilon^{280} = 54.4\ mM^{-1}cm^{-1}$ (29), flash frozen, and stored at −80 °C.

An expression plasmid for the W280A variant was generated from the pET-28b plasmid for $APE1^{\Delta N38}$ (27) using the QuikChange II site-directed mutagenesis kit (Stratagene) with PCR primers of 5′-GAA TGC TCG ATC CAA GAA TGT TGG TGC GCG CCT TGA TTA C (forward), and 5′-GTA ATC AAG GCG CGC ACC AAC ATT CTT GGA TCG AGC ATTC (reverse). The W280A mutation was confirmed by DNA sequencing. $APE1^{\Delta N38}$-W280A was expressed and purified as above, and quantified by absorbance ($\varepsilon^{280} = 50.9\ mM^{-1}cm^{-1}$).

Uniformly ^{15}N-labeled protein was produced by expression in MOPS minimal media with 99% [^{15}N]-NH_4Cl (1g/L) (Cambridge Isotope Laboratories) (30). Briefly, transformed BL21 (DE3) cells (Novagen) were grown overnight on an LB plate (37 °C), then ~30 colonies were used to inoculate 0.2 L of LB medium, and grown (37 °C) to $OD_{600} = 0.6$. Cells were harvested, suspended in 2 l of MOPS minimal media, and grown to $OD_{600} = 0.7$. The temperature was reduced to 15 °C, protein expression was induced with IPTG (0.4 mM) overnight (~14 hrs), and protein was purified as described above.

Human p50, one subunit of the NF-κB heterodimer, was expressed in *E. coli* BL21 (DE3) cells using a pET-14b plasmid (19) with 0.4 mM IPTG for 16 hrs at 16 °C, and purified using nickel affinity (Qiagen) and cation exchange chromatography, as described above for APE1. Purified p50 was dialyzed versus 20 mM HEPES pH 7.9, 0.1 M KCl, 10% glycerol, 0.2 mM EDTA, the p50 concentration was determined using a molar absorption coefficient of $\varepsilon^{280} = 29.3\ mM^{-1}cm^{-1}$, and aliquots were flash frozen and stored at −80 °C.

The oligodeoxynucleotides (ODN) used to make duplex DNA for the APE1 repair and redox assays were synthesized (trityl-on) at the Keck Foundation Biotechnology Resource Laboratory, Yale University. The ODNs were purified with Glen-Pak cartridges (Glen Research) and their concentration was determined by absorbance (31). Duplex DNA was hybridized by heating to 80 °C followed by slow cooling to room temperature. DNA containing a p50 binding site was comprised of 5′-AAGGGACTTTCCGCTGGGGATTCCAY, where Y is fluorescein-dT, and its complement 5′-ATGGAATCCCCAGCGGAAAGTCCCTT. For the AP endonuclease assay, duplex DNA was comprised of 5′-AGTGCGTCC*F*CGACGAC, where *F* is a tetrahydrofuran abasic site analog, and its complement, 5′-GTCGTCGGGGACGCACT.

E3330

(*E*)-3-[2-(5,6-dimethoxy-3-methyl-1,4-benzoquinonyl)]-2-nonylpropenoic acid (E3330), generously provided by Dr. Hiroshi Handa (Tokyo Institute of Technology) or obtained

from Sigma, was dissolved in ethanol-D_6 (99% D) at a concentration of 50 mM and stored at −20 °C.

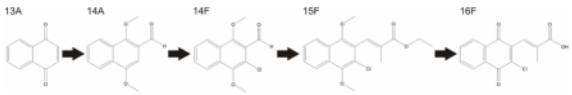

Synthesis of RN7-60

We synthesized a previously identified inhibitor of APE1 redox activity, referred to as RN7-60 or as **16f**, (*E*)-3-(3-chloro-1,4-naphthoquinon-2-yl)-2-methylpropenoic acid, essentially as described (21) but with the changes noted below. Note that compounds **14a**, **15a**, **15f** below are precursors for the synthesis of **16f** as previously described (21). To obtain **14a**, 1, 4-dimethoxy-2-naphthaldehyde (**13a**) (10.0 g, 63.2 mmol) was hydrogenated using Pd/C (10 wt % 0.99 g) in the presence of anhydrous THF (250 mL) at 30 psi for 4 h, at which point it was purified using flash chromatography eluting with CH_2Cl_2, to yield **14a** as a yellow-orange solid (2.26 g, 10.45 mmol, 77%). In an analogous fashion, **14f** was obtained as yellow solid (1.44 g, 5.74 mmol, 64%). ^{1}H NMR ($CDCl_3$): δ 4.00 (s, 3H), 4.06 (s, 3H), 7.59–7.61 (m, 1H), 7.68–7.72 (m, 1H), 8.12–8.14 (m, 1H), 8.23–8.25 (m, 1H), 10.62 (s, 1H). Synthesis of **15f** was as described (21). Following purification using a silica-based gravity column (wash, 100% hexane; elute, 5% EtOAc/95% hexane) and preparative TLC (acetone eluent), afforded **15f** as a yellow solid (150 mg,0.45 mmol,10%). ^{1}H NMR ($CDCl_3$): δ1.41 (t, 3H), 1.80 (s, 3H), 3.81 (s, 3H), 3.94 (s, 3H), 4.21–4.26 (m, 2H), 7.52–7.63 (m, 2H), 7.71–7.72 (d, 1H), 8.11–8.32 (m, 2H). In a similar manner as previously described (21), **16f** was synthesized and purified using preparative TLC eluting with (3:17 acetone: hexanes; 0.5% AcOH, to give a tan solid (11 mg, 0.04 mmol, 7%). ^{1}H NMR ($CDCl_3$): δ 1.25 (d, 3H), 7.26 (d, 1H), 7.81–7.83 (m, 2H), 8.19–8.24 (m, 2H). **16f** was dissolved in ethanol-D_6 (99% D) at a concentration of 50 mM and stored at −20 °C.

NMR experiments and determination of dissociation constants

NMR samples (0.30 ml) contained uniformly ^{15}N-labeled protein (APE1, APE1$^{\Delta N38}$, or APE1$^{\Delta N38}$-W280A) at a concentration of 75–200 μM, in the absence or presence of inhibitor (varying concentrations). The standard NMR buffer contained 0.02 M sodium phosphate pH 6.5, 0.1 M NaCl, 0.5 mM DTT, 0.2 mM EDTA, 10% D_2O, and up to 2% (v/v) ethanol-D_6. Ethanol-D_6 was used to maintain ligand solubility. All samples with ligand were compared to a control that lacked ligand but had an identical concentration of protein and ethanol-D_6. The ^{15}N-HSQC or ^{15}N-TROSY experiments were collected on 600 or 800 MHz Bruker NMR spectrometers, processed with NMRPipe (32), and analyzed with SPARKY (33). The chemical shift change (Δ δ) was calculated using eq. 1, which reflects the total weighted change in ^{1}H and ^{15}N chemical shift for a given peak in the 2D spectra:

$$\Delta\delta=[(\Delta\delta_H)^2+(0.1\Delta\delta_N)^2]^{1/2} \quad (1)$$

We calculated dissociation constants (K_d) from the dependence of Δδ on ligand concentration using DynaFit (34, 35), with global fitting of data for multiple residues. Figures for K_d were generated using Grafit 5 (36).

NMR Saturation Transfer Difference Experiments

^{15}N-labeled APE1$^{\Delta N38}$ was lyophilized and then suspended in NMR buffer (above) prepared with D_2O (99.9% D). The NMR sample (0.5 ml) contained 50 μM APE1$^{\Delta N38}$ and 1 mM E3330 in this buffer with 2% ethanol-D_6. The saturation transfer difference (STD)

NMR experiments were performed as previously described (37) at 600 MHz and 25 °C. The pre-saturation period (2 s) consisted of 40 selective pulses of 50 ms duration and separated by a 1 ms delay. The selective pulse was set for on- and off-resonance frequencies of −0.4 ppm and 30 ppm, respectively. A control STD spectrum collected without the $T_{1\rho}$ filter (30 ms spin-lock pulse) gives the expected 1D spectrum for APE1$^{\Delta N38}$. The ^{1}H and ^{13}C chemical shift assignments for E3330 were confirmed by 1D ^{1}H and 2D ^{13}C-HMBC spectra.

Docking Studies

The molecular docking experiments were performed using AutoDock Vina (38). A crystal structure of APE1 (including residues 44–318; PDBID 1BIX) was prepared for docking using AutoDock Tools (ADT, version 1.5.4) (39), by adding hydrogens, removing metal ions, assigning AD4 atom types, calculating gasteiger charges, and merging non-polar hydrogens. The molecule was allowed no side chain flexibility before formatting into the. pdbqt file. The 3D structure of E3330 was created using ChemBioOffice 2010 and formatted using the ADT program (to add hydrogens, determine AD4 atom types, and calculate partial charges). The ligand was allowed 12 rotatable bonds before final formatting into the. pdbqt format. Global docking of E3330 utilized a 60 Å cube that encompassed the entire protein, and local docking used a 20 Å cube centered at the binding site determined by NMR, giving essentially the same docking result. The exhaustiveness parameter was extended to 100 to enhance the accuracy of predicted binding conformations. A similar approach was used for molecular docking of RN7-60. All docking figures were generated with PyMOL (40).

AP endonuclease assay for APE1

The AP endonuclease activity of APE1 (1 nM) or APE1$^{\Delta N38}$ (2.5 nM) was determined under steady-state conditions with abasic DNA substrate (1 μM) in the presence or absence of E3330 (100 μM). Reactions were performed at 37 °C for APE1 or at 30 °C for APE1$^{\Delta N38}$ in HEMN.1 buffer (0.02 M HEPES pH 7.5, 0.2 mM EDTA, 2.5 mM $MgCl_2$, 0.1 M NaCl). Reactions were initiated by adding concentrated enzyme to buffer containing substrate, with or without E3330, and samples were removed at varying time-points and quenched with 0.1 M NaOH, 0.01 M EDTA (final concentration). All reactions (with or without E3330) contained 2 % ethanol, as needed to maintain solubility of E3330. The reaction progress (product concentration) for each sample was determined by analytical HPLC, as described (31). Initial velocities (v_0) were determined by fitting the data (product concentration versus time) using linear regression, and were converted to k_{obs} (= v_0/[enzyme]).

Redox Assay

Electrophoretic mobility shift assays (EMSAs) were performed using purified APE1 or APE1$^{\Delta N38}$ and p50, essentially as described (20). Briefly, p50 was reduced by incubation in p50 storage buffer (0.02 M HEPES, pH 7.9, 0.1 M KCl, 0.2 mM EDTA, 10% glycerol) with 1 mM tris(2-carboxyethyl)phosphine (TCEP; Calbiochem) for 30 min at 16 °C, and p50 was oxidized in the same buffer but with 1 mM diamide (Sigma) for 30 min at 16 °C. Both APE1 constructs were reduced in APE1 storage buffer (0.02 M HEPES pH 7.5, 0.2 mM EDTA, 0.1 M NaCl, 1 mM DTT, 1 % glycerol) with 1 mM TCEP. Subsequently, TCEP and diamide was removed by three 10-fold dilutions in p50 buffer and centrifugal concentrators (Amicon). Prior to incubation with p50, APE1 or APE1$^{\Delta N38}$ (20 μM) was incubated, in the presence or absence of E3330 (varying concentration), for 5 min at room temperature in binding buffer (0.02 M HEPES pH 7.9, 0.1 M KCl, 0.2 mM EDTA, 5% glycerol, 0.01% NP-40, 0.2 mg/ml BSA) that also contained 2 % ethanol for all samples. Subsequently, oxidized p50 was added (1.5 μM final concentration) and samples were incubated 5 min at 37 °C (APE1) or 30 °C (APE1$^{\Delta N38}$). Finally, p50 DNA (0.1 uM) and poly(dI-dC) (0.15 mg/ml; Sigma) were added and samples were incubated 20 min at room temperature. Samples were diluted 5-fold with TBE sample buffer, 5 ul was loaded to a pre-equilibrated 6%

polyacrylamide native gel (Invitrogen), and electrophoresis was performed with 0.5 X TBE for 65 min at 4 °C. The fluorescein-labeled p50 DNA was detected using a Typhoon 9400 imager.

RESULTS

NMR Determination of the E3330 binding site for APE1

Given the high sensitivity of backbone amide ^{1}H-^{15}N resonances to structural and environmental changes, NMR chemical shift perturbation experiments are a powerful and widely used method to identify ligand binding sites of proteins (41, 42). We previously assigned the backbone and Cβ chemical shifts for human APE1 $^{\Delta N38}$ (27), allowing us to map chemical shift changes induced by ligand binding to existing crystal structures of APE1 (12, 13). The N-terminal region of APE1 (~45 residues) is disordered and yields intense NMR signals that can obscure peaks for some residues in the folded domain. Accordingly, we used an APE1 construct lacking the initial 38 N-terminal residues (APE1 $^{\Delta N38}$) for most of the NMR experiments in this work. Previous studies indicate the 40 N-terminal residues are dispensable for the repair and redox activity of APE1 (43). Nevertheless, because the backbone ^{1}H-^{15}N shifts for nearly all residues of the folded domain are not perturbed by the presence of the N-terminal region (i.e., shifts for APE1 $^{\Delta N38}$ are largely unchanged for APE1), we could readily confirm the ligand binding site for full-length APE1.

To determine the binding site for E3330, we collected ^{15}N-TROSY experiments for APE1 $^{\Delta N38}$, alone and in the presence of E3330 at molar ratios ranging from 0.5:1 to 12:1 (E3330:APE1 $^{\Delta N38}$). Fig. 1A shows overlaid spectra for APE1 $^{\Delta N38}$ alone (black peaks) and APE1 $^{\Delta N38}$ with a 12-fold excess of E3330 (red peaks). Fig. 1B shows closeup views of E3330-induced chemical shift changes for some of the more perturbed residues. As shown in Fig. 1C, substantial chemical shift changes ($\Delta\delta > 0.02$ ppm) are observed for many residues, including G231, M270, M271, N272, A273, V278, W280, and D308, and significant changes ($\Delta\delta > 0.01$ ppm) occur for many additional residues.

Fig. 2 shows a crystal structure of DNA-bound APE1, with the residues most substantially perturbed by E3330 binding ($\Delta\delta > 0.02$ ppm) in stick format. Remarkably, the NMR data reveal that E3330, an inhibitor of *redox* activity, binds in a pocket of the DNA-binding cleft for the repair activity of APE1. Indeed, the residues exhibiting substantial E3330-induced shift changes also function in the repair activity, by interacting directly with bound AP-DNA substrate or lining the DNA binding cleft. The two residues most perturbed by E3330 binding (G231, W280) lie within 5 Å of the flipped abasic nucleotide in the enzyme-substrate complex. While the E3330 binding site is clearly in the DNA-binding cleft, it is adjacent to, but distinct from, the catalytic site that contains residues essential for phosphodiester bond cleavage (E96, Y171, D210, N212, H309). While many previous studies suggested a conserved cysteine residue, C65, is essential for APE1 redox activity, we observe *no chemical shift changes* for C65 upon binding E3330 (Fig. 1). Likewise, we find no E3330-induced shift changes for C93, also implicated in redox activity, or any other Cys residue.

E3330 Binding Site Predicted by Molecular Docking

We modeled the E3330 binding using a crystal structure of APE1 and the docking program AutoDock Vina (44), a more robust and accurate version of AutoDock 4 (38). We used three-dimensional search fields that encompassed the entire protein for global docking, or a specific region that included the residues exhibiting substantial E3330-induced shift perturbations ($\Delta\delta > 0.02$ ppm) for local docking. The ten most energetically favorable docking results, for both local and global docking, place E3330 in the DNA-binding cleft at

the site determined by the NMR experiments (Fig. 2B and 2C). Indeed, some residues exhibiting the largest E3330-induced shift perturbation (G231, W280) lie within 5 Å of the docked E3330 molecule. Thus, the docking studies are fully consistent with the binding site determined by NMR.

Binding Parameters and Potential Effects of Mg^{2+} and pH

Fig. 3A shows a plot of chemical shift perturbation (Δδ) versus E3330 concentration for several residues exhibiting E3330-induced shift changes for APE1 $^{\Delta N38}$. We globally fit the data (Δδ versus [E3330]) for all of these residues using the program DynaFit (34, 35), obtaining a dissociation constant of K_d = 390 ± 60 μM. Given that the E3330 binding site is in the DNA cleft and therefore relatively close to the coordination site of the Mg^{2+} cofactor (required for repair activity), we repeated the E3330 NMR titration using the same NMR buffer, but with $MgCl_2$ (2 mM). We find that the same residues participate in E3330 binding, and global fitting of Δδ versus [E3330] for several of the perturbed resonances shows the binding affinity is nearly the same, K_d = 610 ± 99 μM (Fig. 3B). We also performed the E3330 titration in buffer without phosphate (which could bind the DNA cleft) and with neutral pH and Mg^{2+}, and we found that the same residues mediate E3330 binding and the affinity is essentially the same, K_d = 520 ± 248 μM (not shown). Consistent with relatively weak binding for E3330, the data in Fig. 1B shows the binding is in fast exchange on the NMR timescale, $k_{ex} \gg 2\pi\Delta\nu$ = ~100 s^{-1}, as indicated by observation of a single averaged peak for the free and bound states (45). Our results are consistent with the recent findings that E3330 binding to APE1 $^{\Delta N40}$ is relatively weak (46) but not consistent with the proposal that binding is *exceedingly slow* (k_{on} = 0.02 $M^{-1}s^{-1}$; k_{off} = 10^{-4} s^{-1}), which would be slow on the NMR timescale (i.e., $k_{ex} \ll 2\pi\Delta\nu$) and be expected to yield individual peaks for the free and E3330-bound states.

E3330 Binding to Full Length APE1

We also collected NMR shift perturbation experiments for full-length APE1, to ascertain whether E3330 binding might be altered by presence of its disordered N-terminal region. These experiments were performed at 35 °C, which serves to suppress the intense signals from residues in the N-terminal region, and is more physiologically relevant. The residues experiencing E3330-induced shift perturbation for APE1 are also perturbed for APE1 $^{\Delta N38}$, indicating E3330 binds the same site for both proteins (Fig. S1 of Supporting Information). NMR shift perturbations were used to calculate the binding affinity of APE1 for E3330, giving K_d = 55 ± 12 μM, about 7-fold tighter than the K_d for E3330 binding to APE1$^{\Delta N38}$ at 25 °C. NMR data for binding of E3330 to full-length APE1 at 25 °C indicates the binding affinity is close to that observed for APE1$^{\Delta N38}$ at 25 °C (not shown). Thus, tighter binding of E3330 to APE1 at 35°C versus 25 °C appears to be an effect of temperature rather than presence of the N-terminal region, consistent with the absence of E3330-induced shift changes for N-terminal residues of APE1. The K_d = 55 μM determined here for E3330 binding to full-length APE1 (at 37 °C) is similar to recently reported IC_{50} values for inhibition of APE1 redox activity by E3330 (17, 22).

Saturation Transfer Difference NMR Experiments

To further characterize the binding of E3330 to APE1, we performed saturation transfer difference (STD) NMR experiments, an established approach for identifying regions of a ligand that are located at the protein-ligand interface (37). STD experiments monitor the transfer of saturation from ^{1}H resonances of the protein to ^{1}H resonances of the ligand, following selective saturation of the protein. The approach is well suited for protein-ligand interactions that are relatively weak (0.01 μM < K_d < 1000 μM) and in rapid exchange (37), consistent with our observed parameters for E3330 binding to APE1 (Figs. 1, 3). As shown in Fig. 4, an STD NMR spectrum indicates that nearly all ^{1}H resonances of E3330

participate to some extent in binding APE1, consistent with the nearly complete burial of E3330 in a pocket of the DNA binding cleft, as indicated by NMR shift perturbations and predicted by molecular docking (Fig. 2).

APE1 W280A Mutant Binds E3330

The large E3330-induced shift perturbation for W280 (Fig. 1) suggests it may participate in binding E3330, and we sought to examine this idea using a W280A mutant. We prepared an expression plasmid for APE1 $^{\Delta N38}$-W280A and produced ^{15}N-labeled protein using the approach for wild-type enzyme. As expected, a ^{15}N-HSQC spectrum for APE1 $^{\Delta N38}$-W280A lacks the peak for the side-chain N-H of W280, confirming its assignment, and the backbone N-H peak is dramatically shifted (Fig. S2 of Supporting Information). The spectrum also shows that backbone amide N-H resonances of many residues are perturbed by the W280A mutation, and that the protein is properly folded. We collected NMR shift perturbation experiments for E3330 binding to APE1 $^{\Delta N38}$-W280A (Fig. 5A and Fig. S3 of Supporting Information). Despite the significant structural changes imparted by the mutation, the residues most perturbed by E3330 binding to APE1 $^{\Delta N38}$-W280A (G231, Y269, M270, M271, A273, and D308) are consistent with those perturbed for wild-type enzyme. Thus, the binding site for E3330 is not substantially changed by the W280A mutation. To allow docking studies of E3330 to APE1 $^{\Delta N38}$-W280A, we used the program COOT (Crystallographic Object-Oriented Toolkit (COOT) (47) to generate the W280A mutation in an APE1 crystal structure. Using this structural model, docking studies (AutoDock Vina) predict E3330 binds APE1-W280A at the same site identified by NMR. Moreover, E3330 binds the W280A mutant at essentially the same site as for wild-type APE1, though E3330 appears to be more buried for W280A relative to wild-type protein (Fig. 5B). Consistent with this observation, the binding affinity of APE1 $^{\Delta N38}$-W280A for E3330, K_d = 107 ± 22 μM, is about 4-fold tighter than the affinity for wild-type APE1 $^{\Delta N38}$ (Fig. 5) (conditions of 25 °C, pH 6.5, no Mg^{2+}).

E3330 inhibits the repair and redox activity of APE1

Given our unexpected finding that E3330 binds the repair active-site of APE1, we examined the effect of E3330 on the DNA repair and redox activities of APE1. We find that E3330 substantially inhibits the AP endonuclease of APE1 $^{\Delta N38}$ (Fig. 6A) and full-length APE1 (Fig. 6B). Indeed, steady-state kinetics experiments show APE1 $^{\Delta N38}$ activity, k_{obs} = 0.53 ± 0.02 s^{-1}, is reduced 40% by E3330 at a 100 μM concentration, k_{obs} = 0.29 ± 0.02 s^{-1}. Likewise, repair activity of full-length APE1, k_{obs} = 0.39 ± 0.01 s^{-1}, is 3-fold lower in the presence of 100 μM E3330, k_{obs} = 0.13 ± 0.01 s^{-1}. While this result stands in contrast with previous reports that E3330 does not inhibit the AP endonuclease activity of APE1 (17, 22), it is entirely consistent with the E3330 binding site determined here by NMR and supported by molecular docking.

We also examined the effect of E3330 on the redox activity of APE1 using an electrophoretic mobility shift assay (EMSA) (20). As shown in Fig. 6C, we find that APE1 and APE1 $^{\Delta N38}$ can activate DNA binding of oxidized p50 (redox-sensitive subunit of NF-κB), and that E3330 inhibits this activity for both APE1 constructs. These results are consistent with previous reports that E3330 inhibits the ability of APE1 to activate oxidized p50 (using purified recombinant proteins rather than cell extracts) (19, 20).

Binding Site for RN7-60

To characterize the binding of a structurally distinct inhibitor of APE1 redox activity, we synthesized a naphthoquinone analog of E3330 known as RN7-60 (or **16f**); (*E*)-3-(3-chloro-1,4-naphthoquinon-2-yl)-2-methylpropenoic acid (21, 22). We synthesized RN7-60 using a previously described approach (21) with some modifications (Materials and

Methods), and verified the purity and structure by thin layer chromatography and NMR. As shown in Fig. 7A, NMR shift perturbation experiments reveal that RN7-60 binds APE1 $^{\Delta N38}$ at a site that involves R136 and Q137. The binding affinity of APE1 $^{\Delta N38}$ for RN7-60, K_d = 264 ± 72 μM (Fig. 7B) is about 2-fold tighter than for E3330 (under similar conditions). The most energetically favorable binding site for RN7-60 predicted by molecular docking (AutoDock Vina) is fully consistent with the site determined by NMR (Fig. 7C), on the opposite side of APE1 relative to the E3330 site (Fig. 7C). We find no evidence for covalent modification of any Cys residue by RN7-60 under the conditions used here (which include 0.5 mM DTT). This observation suggests previous findings that RN7-60 forms adducts with all seven Cys residues of APE1(22) could reflect the absence of any reducing agent and perhaps low ionic strength of the reaction buffer (10 mM HEPES). We find APE1 precipitates under such conditions (even at 4 °C), suggesting a loss of structural integrity due to low ionic strength and perhaps lack of reducing agent, whereas it is highly stable in the conditions used here.

DISCUSSION

Using NMR and molecular docking methods, we identified the binding site for E3330 and RN7-60, providing the first structural information for any inhibitor of APE1 redox activity. RN7-60 binds a pocket on the opposite side of the protein from E3330, and seems to interact with Arg136 and Gln137 (Fig. 7). Observation that E3330 and RN7-60 bind different locations of APE1, while not necessarily expected since they are both redox inhibitors, is consistent with significant structural differences between these compounds. The RN7-60 binding site is removed from C65 (~15 Å), and RN7-60 binding induces no chemical shift perturbations for C65 or any other Cys, including C138, which is close to the binding site. Thus, the previous finding that RN7-60 can form a covalent adduct with buried Cys residues of APE1 (22) seems likely to be due to experimental conditions (0.01 M HEPES pH 7.5, no salt or reducing agent). Our results do not support the proposal that RN7-60 causes partial unfolding of APE1, thereby exposing buried Cys residues (22).

Remarkably, the NMR and docking studies here show that E3330 binds a pocket in the DNA-binding cleft for the repair activity of APE1 (Fig. 2), far removed from C65, a residue suggested by some studies to be required for redox activity (11, 16, 17). The specificity of E3330 for the DNA-binding cleft is further demonstrated by observation that its affinity is enhanced by removal of the W280 side chain (Fig. 5). It appears the W280A mutation provides additional space and interactions that facilitate E3330 binding, as indicated by a 4-fold lower K_d for W280A relative to wild-type APE1.

Binding of E3330 in the DNA repair active site is also supported our finding that E3330 can substantially inhibit the AP endonuclease activity of APE1; activity is reduced by 67 % for an E3330 concentration of 100 μM at 37 °C (Fig. 6). This level of inhibition is consistent with binding affinity of E3330 for APE1, K_d = 55 ± 12 μM at 35 °C (Fig. S1 of Supporting Information). Importantly, this finding suggests E3330 is not a selective inhibitor of APE1 redox activity, as previously proposed (16, 17). Cell-based studies that employ E3330 to inhibit APE1 redox activity report that observed effects occur for E3330 concentrations ranging from 5–50 μM (15, 17, 21, 23, 48). Thus, our findings raise the possibility that the effects of E3330 treatment could include inhibition of APE1 repair activity. To our knowledge, this possibility has not been carefully examined in cell-based studies, indicating additional studies are needed to determine the extent to which E3330 may inhibit APE1 repair activity in cells.

While the mechanism by which E3330 inhibits APE1 redox activity remains unknown, our findings are not consistent with three recent proposals. A study using mass spectrometry and

chemical modification (N-methylmaleimide or NEM) reported that E3330 promotes NEM modification of at least one buried Cys in APE1 $^{\Delta N40}$ and then rapid modification of the four remaining buried Cys residues (46). NEM modification was reportedly much slower for buried relative to solvent-exposed Cys residues ($t_{1/2}$ of 7 h and 2 m, respectively). It is concluded that NEM modification is limited by slow association of E3330 and APE1 $^{\Delta N40}$ and proposed that E3330 binds selectively to locally unfolded (LU) APE1 $^{\Delta N40}$ and traps the LU state, allowing NEM modification of a (formerly) buried Cys (46). The reported NEM data and binding model yield exceedingly slow binding kinetics; k_{on} = 0.02 $M^{-1}s^{-1}$, k_{off} = 10^{-4} s^{-1} (i.e., half-life of 2 h for dissociation). Moreover, the model seems inconsistent with their finding that, after incubation with E3330 for 24 h, APE1 exhibits no NEM modification in 30 m (for buried Cys). In contrast, our NMR data shows that binding of E3330 to APE1 is rapid; the exchange rate is much greater than the chemical shift difference for free and ligand-bound states ($k_{ex} = k_{on}[L] + k_{off} \gg 2\pi\Delta\nu \approx 100\ s^{-1}$). Thus, the report that E3330 enhances NEM modification of APE1 could reflect an E3330-induced conformation that provides minimal access of NEM to a buried Cys and which is likely to be sparsely populated and/or have a short lifetime. NMR studies of APE1 dynamics, in the presence and absence of E3330, could address this possibility (45).

It was also proposed that E3330 promotes solvent exposure of C65, based on NEM modification of buried Cys residues (including C65) (46). However, because the mass spectrometry data do not indicate which buried Cys is modified first, it would seem the results could be explained by E3330-induced exposure of a Cys other than C65, trapping an "open" conformation that allows subsequent modification of the other buried Cys residues (including C65). Indeed, this possibility is demonstrated by NEM modification of the buried Cys residues for the C65A mutant (46). Our NMR results provide no evidence that E3330 binding leads to a significantly populated conformation in which C65 (or any buried Cys) is exposed, although E3330 could alter the dynamics of APE1 which might transiently expose a buried Cys residue.

Our results do not support the proposal that E3330 inhibits redox activity by promoting the formation of disulfide bonds in APE1 (46). It was reported that incubation of APE1 $^{-N40}$ with E3330 leads to formation of a C65-C93 disulfide bond, and several other disulfides (C65-C99, C65-C138, C93-C99, C93-C138), involving S nuclei that are separated by 8-20 Å in APE1 (12). Notably, a C93-C208 disulfide was not reported, even though they are separated by only 3.5 Å. However, the relatively minor E3330-induced chemical shift changes observed here (Fig. 1) are not consistent with the dramatic conformational change that would be needed to form these disulfide bonds, and no Cys residue is perturbed by E3330 binding, at 25 °C (APE1 $^{\Delta N38}$) or 35°C (APE1). One potential explanation for the previous results is that they arise from experimental conditions (37°C, 0.01 M HEPES pH 7.5, no salt or reducing agent). We find the truncated enzyme (APE1 $^{\Delta N38}$) aggregates and precipitates rapidly (within 7 m) under these conditions at 37 °C (Fig. S4 of Supporting Information), and this could promote formation of disulfide bonds, particularly in buffer that lacks reducing agent. In contrast, full length APE1 is stable for >1 h at 37 °C (Fig. S4 of Supporting Information).

Our findings suggest some potential mechanisms by which E3330 might inhibit the redox activity of APE1. In a potential redox mechanism where APE1 directly reduces the Cys residue in a transcription factor, which has been shown by only a few studies employing purified proteins rather than cell extracts (19, 20), redox inhibitors could potentially act by blocking productive binding of APE1 to the TF, or perhaps by suppressing an APE1 conformational change needed for TF binding or activation. If C65 or perhaps C93 is involved in direct reduction of the redox-sensitive Cys of the TF, then E3330 and RN7-60 could act as allosteric effectors, since they bind a site removed from C65 and C93. It is

notable that the vast majority of APE1 redox assays reported in the literature employ cell extracts containing the TF (rather than pure TF), raising the possibility that other factors are involved in APE1-mediated TF activation. This possibility is supported by findings that the equivalent of C65 in murine APE1 is not needed for TF activation *in vivo* or cell extracts (14), and by findings that APE1 facilitates TF activation by glutathione (GSH) or thioredoxin (Trx) (15). This "redox chaperone" activity might involve APE1-mediated recruitment of GSH or Trx to the TF, or an APE1-mediated conformational change in the TF that exposes a redox-sensitive Cys to GSH or Trx (15). It is conceivable that E3330 and related compounds could act by blocking APE1 interactions with GSH or Trx, or perhaps with the TF itself.

A detailed explanation for how E3330 and related compounds inhibit APE1 redox activity must await additional studies into the redox mechanism itself. Nevertheless, our results provide the first direct structural information for any APE1 inhibitor, and could facilitate the design and optimization of improved inhibitors that could eventually lead to compounds useful for research and perhaps clinical purposes. However, our findings suggest that obtaining inhibitors that are highly selective for the redox or repair activities of APE1 may be more challenging than previously envisioned.

Supplementary Material

Refer to Web version on PubMed Central for supplementary material.

Acknowledgments

This work was supported by a grant from the NIH (GM72711 to A.C.D.). B.A.M. was supported by a Chemistry-Biology Interface (CBI) Training grant from the NIH (T32-GM066706).

We thank Hiroshi Handa and Satoshi Hirao (Tokyo Institute of Technology) for providing a sample of E3330 and a plasmid for expressing p50, and Kristen Varney (University of Maryland School of Medicine) and Kellie Hom (NMR Facility, University of Maryland School of Pharmacy) for assistance with collecting NMR data.

Abbreviations

APE1	apurinic/apyrimidinic endonuclease 1
E3330	(*E*)-3-[2-(5,6-dimethoxy-3-methyl-1,4-benzoquinonyl)]-2-nonylpropenoic acid
HSQC	heteronuclear single quantum coherence
RN7-60	(*E*)-3-(3-chloro-1,4-naphthoquinon-2-yl)-2-methylpropenoic acid
STD	saturation transfer difference
TROSY	transverse relaxation optimized spectroscopy

References

1. Robson CN, Hickson ID. Isolation of cDNA clones encoding a human apurinic/apyrimidinic endonuclease that corrects DNA repair and mutagenesis defects in E. coli xth (exonuclease III) mutants. Nucleic Acids Res. 1991; 19:5519–5523. [PubMed: 1719477]
2. Demple B, Herman T, Chen DS. Cloning and expression of APE, the cDNA encoding the major human apurinic endonuclease: definition of a family of DNA repair enzymes. Proc Natl Acad Sci U S A. 1991; 88:11450–11454. [PubMed: 1722334]
3. Hegde ML, Hazra TK, Mitra S. Early steps in the DNA base excision/single-strand interruption repair pathway in mammalian cells. Cell Res. 2008; 18:27–47. [PubMed: 18166975]

4. Okazaki T, Chung U, Nishishita T, Ebisu S, Usuda S, Mishiro S, Xanthoudakis S, Igarashi T, Ogata E. A redox factor protein, ref1, is involved in negative gene regulation by extracellular calcium. J Biol Chem. 1994; 269:27855–27862. [PubMed: 7961715]
5. Bhakat KK, Mantha AK, Mitra S. Transcriptional Regulatory Functions of Mammalian AP-Endonuclease (APE1/Ref-1), an Essential Multifunctional Protein. Antioxid Redox Signal. 2009; 11:621–637. [PubMed: 18715144]
6. Xanthoudakis S, Smeyne RJ, Wallace JD, Curran T. The redox/DNA repair protein, Ref-1, is essential for early embryonic development in mice. Proc Natl Acad Sci U S A. 1996; 93:8919–8923. [PubMed: 8799128]
7. Izumi T, Brown DB, Naidu CV, Bhakat KK, Macinnes MA, Saito H, Chen DJ, Mitra S. Two essential but distinct functions of the mammalian abasic endonuclease. Proc Natl Acad Sci U S A. 2005; 102:5739–5743. [PubMed: 15824325]
8. Fung H, Demple B. A vital role for Ape1/Ref1 protein in repairing spontaneous DNA damage in human cells. Mol Cell. 2005; 17:463–470. [PubMed: 15694346]
9. Xanthoudakis S, Curran T. Identification and Characterization of Ref-1, a Nuclear-Protein That Facilitates Ap-1 DNA-Binding Activity. EMBO J. 1992; 11:653–665. [PubMed: 1537340]
10. Xanthoudakis S, Miao G, Wang F, Pan YC, Curran T. Redox activation of Fos-Jun DNA binding activity is mediated by a DNA repair enzyme. EMBO J. 1992; 11:3323–3335. [PubMed: 1380454]
11. Walker LJ, Robson CN, Black E, Gillespie D, Hickson ID. Identification of residues in the human DNA repair enzyme HAP1 (Ref-1) that are essential for redox regulation of Jun DNA binding. Mol Cell Biol. 1993; 13:5370–5376. [PubMed: 8355688]
12. Gorman MA, Morera S, Rothwell DG, de La Fortelle E, Mol CD, Tainer JA, Hickson ID, Freemont PS. The crystal structure of the human DNA repair endonuclease HAP1 suggests the recognition of extra-helical deoxyribose at DNA abasic sites. EMBO J. 1997; 16:6548–6558. [PubMed: 9351835]
13. Mol CD, Izumi T, Mitra S, Tainer JA. DNA-bound structures and mutants reveal abasic DNA binding by APE1 and DNA repair coordination [corrected]. Nature. 2000; 403:451–6. [PubMed: 10667800]
14. Ordway JM, Eberhart D, Curran T. Cysteine 64 of Ref-1 is not essential for redox regulation of AP-1 DNA binding. Mol Cell Biol. 2003; 23:4257–4266. [PubMed: 12773568]
15. Ando K, Hirao S, Kabe Y, Ogura Y, Sato I, Yamaguchi Y, Wada T, Handa H. A new APE1/Ref-1-dependent pathway leading to reduction of NF-kappa B and AP-1, and activation of their DNA-binding activity. Nucleic Acids Res. 2008; 36:4327–4336. [PubMed: 18586825]
16. Georgiadis MM, Luo M, Gaur RK, Delaplane S, Li X, Kelley MR. Evolution of the redox function in mammalian apurinic/apyrimidinic endonuclease. Mutat Res-Fundam Mol Mech Mutagen. 2008; 643:54–63.
17. Luo M, Delaplane S, Jiang A, Reed A, He Y, Fishel M, Nyland RL, Borch RF, Qiao X, Georgiadis MM, Kelley MR. Role of the multifunctional DNA repair and redox signaling protein Ape1/Ref-1 in cancer and endothelial cells: Small-molecule inhibition of the redox function of Ape1. Antioxid Redox Signal. 2008; 10:1853–1867. [PubMed: 18627350]
18. Hiramoto M, Shimizu N, Sugimoto K, Tang JW, Kawakami Y, Ito M, Aizawa S, Tanaka H, Makino I, Handa H. Nuclear targeted suppression of NF-kappa B activity by the novel quinone derivative E3330. J Immunol. 1998; 160:810–819. [PubMed: 9551916]
19. Shimizu N, Sugimoto K, Tang JW, Nishi T, Sato I, Hiramoto M, Aizawa S, Hatakeyama M, Ohba R, Hatori H, Yoshikawa T, Suzuki F, Oomori A, Tanaka H, Kawaguchi H, Watanabe H, Handa H. High-performance affinity beads for identifying drug receptors. Nat Biotechnol. 2000; 18:877–881. [PubMed: 10932159]
20. Nishi T, Shimizu N, Hiramoto M, Sato L, Yamaguchi Y, Hasegawa M, Aizawa S, Tanaka H, Kataoka K, Watanabe H, Handa H. Spatial redox regulation of a critical cysteine residue of NF-kappa B in vivo. J Biol Chem. 2002; 277:44548–44556. [PubMed: 12213807]
21. Nyland RL, Luo M, Kelley MR, Borch RF. Design and synthesis of novel quinone inhibitors targeted to the redox function of apurinic/apyrimidinic endonuclease 1/redox enhancing factor-1 (Ape1/ref-1). J Med Chem. 2010; 53:1200–1210. [PubMed: 20067291]

22. Kelley MR, Luo M, Reed A, Su D, Delaplane S, Borch RF, Nyland RL, Gross ML, Georgiadis MM. Functional Analysis of Novel Analogues of E3330 That Block the Redox Signaling Activity of the Multifunctional AP Endonuclease/Redox Signaling Enzyme APE1/Ref-1. Antioxid Redox Signal. 2011; 14:1387–1401. [PubMed: 20874257]
23. Zou GM, Maitra A. Small-molecule inhibitor of the AP endonuclease 1/REF-1 E3330 inhibits pancreatic cancer cell growth and migration. Mol Cancer Ther. 2008; 7:2012–2021. [PubMed: 18645011]
24. Fishel ML, Colvin ES, Luo M, Kelley MR, Robertson KA. Inhibition of the redox function of APE1/Ref-1 in myeloid leukemia cell lines results in a hypersensitive response to retinoic acid-induced differentiation and apoptosis. Exp Hematol. 2010; 38:1178–1188. [PubMed: 20826193]
25. Jiang A, Gao H, Kelley MR, Qiao X. Inhibition of APE1/Ref-1 redox activity with APX3330 blocks retinal angiogenesis in vitro and in vivo. Vision Res. 2011; 51:93–100. [PubMed: 20937296]
26. Zou GM, Luo MH, Reed A, Kelley MR, Yoder MC. Ape1 regulates hematopoietic differentiation of embryonic stem cells through its redox functional domain. Blood. 2007; 109:1917–1922. [PubMed: 17053053]
27. Manvilla BA, Varney KM, Drohat AC. Chemical shift assignments for human apurinic/apyrimidinic endonuclease 1. Biomol NMR Assign. 2009; 4:5–8. [PubMed: 19888678]
28. Fitzgerald ME, Drohat AC. Coordinating the Initial Steps of Base Excision Repair. Apurinic/apyrimidinic endonuclease 1 actively stimulates thymine DNA glycosylase by disrupting the product complex. J Biol Chem. 2008; 283:32680–32690. [PubMed: 18805789]
29. Gill SC, von Hippel PH. Calculation of protein extinction coefficients from amino acid sequence data. Anal Biochem. 1989; 182:319–326. [PubMed: 2610349]
30. Amburgey JC, Abildgaard F, Starich MR, Shah S, Hilt DC, Weber DJ. 1H, 13C and 15N NMR assignments and solution secondary structure of rat Apo-S100 beta. J Biomol NMR. 1995; 6:171–179. [PubMed: 8589606]
31. Morgan MT, Bennett MT, Drohat AC. Excision of 5-halogenated uracils by human thymine DNA glycosylase: Robust activity for DNA contexts other than CpG. J Biol Chem. 2007; 282:27578–27586. [PubMed: 17602166]
32. Delaglio F, Grzesiek S, Vuister GW, Zhu G, Pfeifer J, Bax A. NMRPipe: a multidimensional spectral processing system based on UNIX pipes. J Biomol NMR. 1995; 6:277–93. [PubMed: 8520220]
33. Goddard, TD.; Kneller, DG. University of California San Francisco. San Francisco:
34. Kuzmic P. Program DYNAFIT for the analysis of enzyme kinetic data: application to HIV proteinase. Anal Biochem. 1996; 237:260–273. [PubMed: 8660575]
35. Kuzmic P. DynaFit--A Software Package for Enzymology. Methods Enzymol. 2009; 467:247–280. [PubMed: 19897096]
36. Leatherbarrow, RJ. Erithacus Software Ltd. Staines, U.K: 1998.
37. Mayer M, Meyer B. Group epitope mapping by saturation transfer difference NMR to identify segments of a ligand in direct contact with a protein receptor. J Am Chem Soc. 2001; 123:6108–6117. [PubMed: 11414845]
38. Trott O, Olson AJ. AutoDock Vina: improving the speed and accuracy of docking with a new scoring function, efficient optimization, and multithreading. J Comput Chem. 2010; 31:455–461. [PubMed: 19499576]
39. Morris GM, Goodsell DS, Halliday RS, Huey R, Hart WE, Belew RK, Olson AJ. Automated Docking Using a Lamarckian Genetic Algorithm and Empirical Binding Free Energy Function. Journal of Computational Chemistry. 1998; 19:1639–1662.
40. DeLano, WL. DeLano Scientific. Palo Alto: 2002.
41. Bonvin A, Boelens R, Kaptein R. NMR analysis of protein interactions. Curr Opin Chem Biol. 2005; 9:501–508. [PubMed: 16122968]
42. Zuiderweg ER. Mapping protein-protein interactions in solution by NMR spectroscopy. Biochemistry. 2002; 41:1–7. [PubMed: 11771996]
43. Izumi T, Mitra S. Deletion analysis of human AP-endonuclease: minimum sequence required for the endonuclease activity. Carcinogenesis. 1998; 19:525–527. [PubMed: 9525290]

44. Trott O, Olson AJ. Software News and Update AutoDock Vina: Improving the Speed and Accuracy of Docking with a New Scoring Function, Efficient Optimization, and Multithreading. J Comput Chem. 2010; 31:455–461. [PubMed: 19499576]

45. Mittermaier AK, Kay LE. Observing biological dynamics at atomic resolution using NMR. Trends Biochem Sci. 2009; 34:601–611. [PubMed: 19846313]

46. Su D, Delaplane S, Luo M, Rempel DL, Vu B, Kelley MR, Gross ML, Georgiadis MM. Interactions of Apurinic/Apyrimidinic Endonuclease with a Redox Inhibitor: Evidence for an Alternate Conformation of the Enzyme. Biochemistry. 2011; 50:82–92.

47. Emsley P, Lohkamp B, Scott WG, Cowtan K. Features and development of Coot. Acta Crystallogr D Biol Crystallogr. 2010; 66:486–501. [PubMed: 20383002]

48. Zou GM, Karikari C, Kabe Y, Handa H, Anders RA, Maitra A. The Ape-1/Ref-1 redox antagonist E3330 inhibits the growth of tumor endothelium and endothelial progenitor cells: therapeutic implications in tumor angiogenesis. J Cell Physiol. 2009; 219:209–218. [PubMed: 19097035]

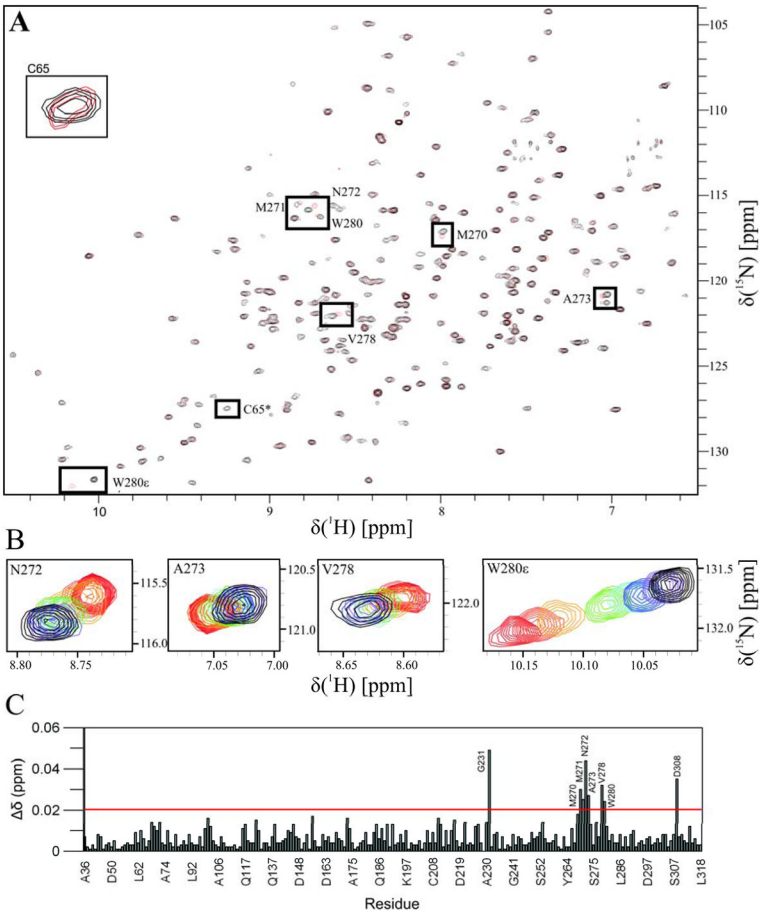

Fig. 1.

E3330-induced chemical shift perturbations for APE1 $^{\Delta N38}$. (A) Overlay of ^{15}N-TROSY spectra for APE1 ^{N38} (76 μM, black peaks) and APE1 $^{\Delta N38}$ with 12-fold excess E3330 (red) collected at 800 MHz, 25 °C. Some of the most strongly perturbed residues are boxed. Note that Cys65 is boxed to indicate it is *not* altered by E3330 binding. (B) Close-up views of ^{1}H-^{15}N shift perturbations for N272, A273, and V278 (backbone) and W280 (side chain), showing data for free APE1 $^{\Delta N38}$ (black) and for E3330:APE1$^{\Delta N38}$ ratios of 0.5:1 (purple), 1:1 (blue), 2:1 (teal), 4:1 (green), 6:1 (yellow), 10:1 (orange), and 12:1 (red). (C) Plot of E3330-induced shift perturbations (Δδ) versus amino acid residue (those with Δδ ≥ 0.02 ppm labeled).

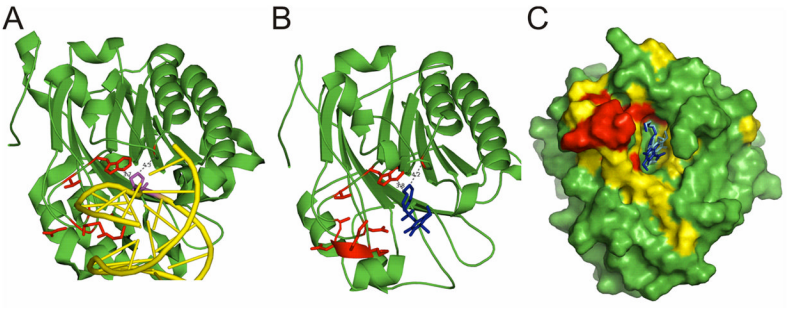

Fig. 2.

E3330 binds in the DNA repair active site of APE1. (A) Residues exhibiting the largest E3330-induced shift perturbations in the spectra from Fig. 1 ($\Delta\delta \geq 0.02$ ppm; G231, M270, M271, N272, A273, V278, W280, D308) are shown in red stick format on an APE1-DNA crystal structure (PDBID: 1DE8). Note that G231 and W280 lie within 5 Å of the flipped abasic sugar (purple) in the APE1-DNA complex. (B) The E3330 binding site predicted by molecular docking is in excellent agreement with NMR shift perturbations. Shown is a docking result for E3330 (blue, stick) bound to APE1 (PDBID: 1BIX), with APE1 oriented as in 2A and the most perturbed residues in red stick format. Note that docked E3330 lies within 5 Å of G231 and W280. (C) Surface representation of APE1 with E3330 bound using global (blue) and local (cyan) docking; residues with larger perturbations ($\Delta\delta \geq 0.02$ ppm) are red and those with significant perturbations ($\Delta\Delta \geq 0.01$ ppm) are yellow. The protein is rotated up (about a horizontal axis) relative to the orientation in A and B for a better view of the binding pocket.

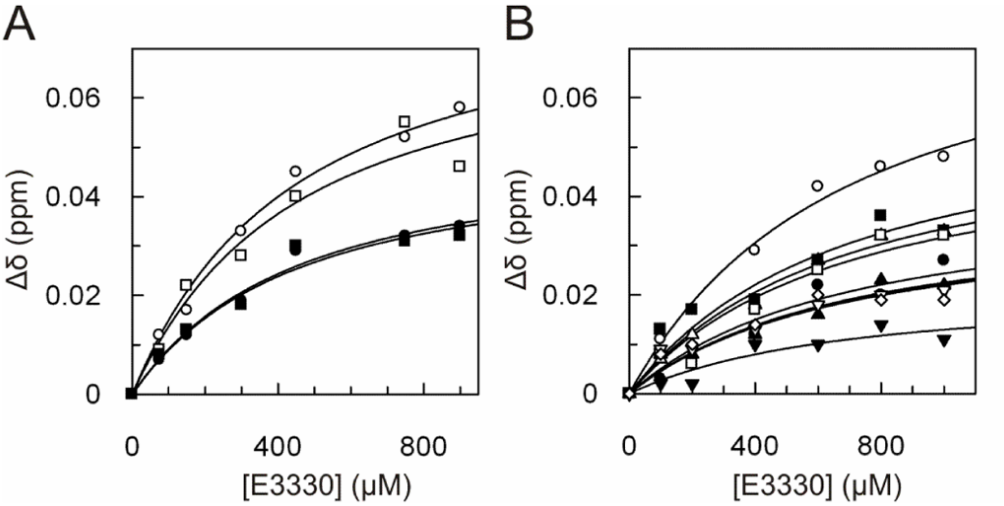

Fig. 3.

Binding affinity of APE1$^{\Delta N38}$ for E3330 determined in buffer without $MgCl_2$ (A) or with 2 mM $MgCl_2$ (B). The E3330 binding affinity was determined from the dependence of shift perturbation (Δδ) on E3330 concentration, using DynaFit and global fitting of data for multiple residues, giving K_d = 390 ± 60 μM for Mg^{2+}-free APE1$^{\Delta N38}$ (A) and K_d = 610 ± 99 μM for Mg^{2+}-bound APE1$^{\Delta N38}$ (B). Fitting included data for N226 (▼), K227 (▽), Y269 (▲), M270 (△), M271 (■), N272 (○), A273 (●), V278 (□), and an unassigned Arg side chain (◇).

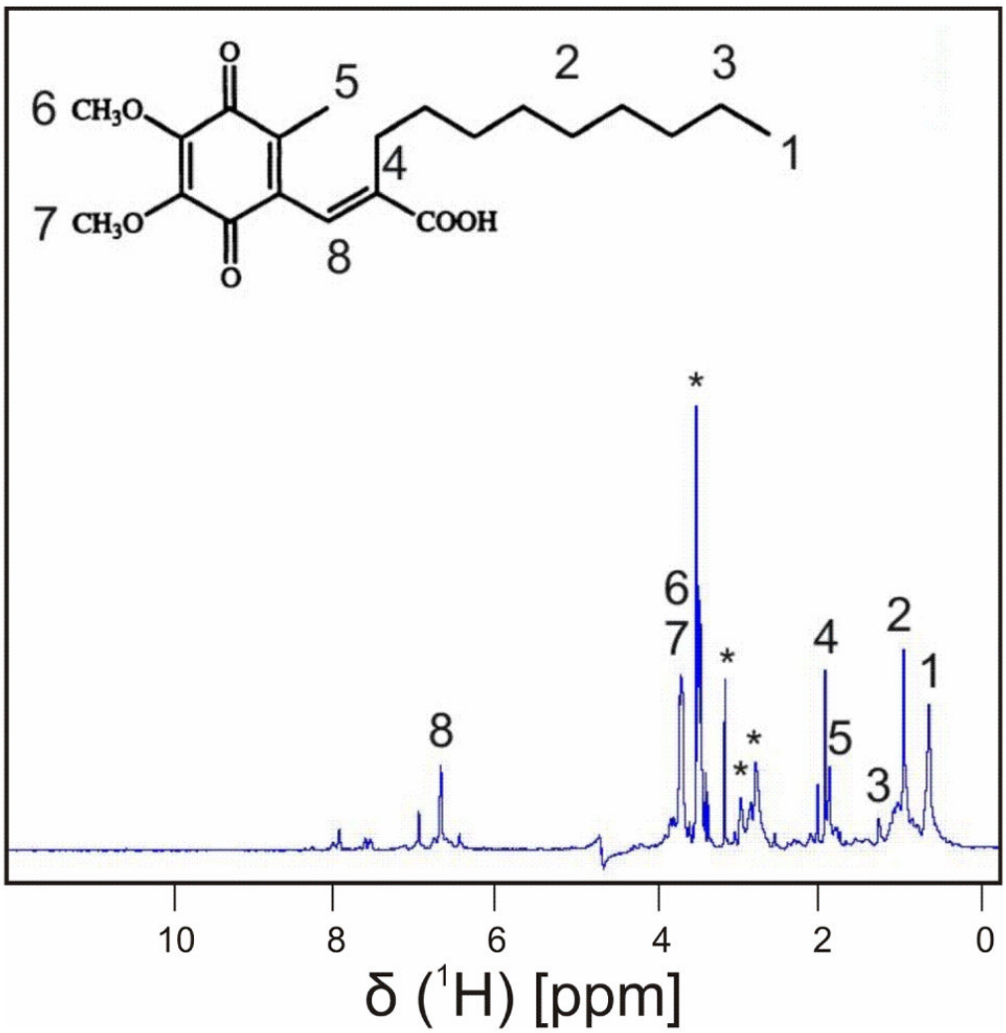

Fig. 4.

Saturation transfer difference (STD) NMR spectrum indicates that all ^{1}H resonances of E3330 interact to some extent with APE1. The structure of E3330 is shown with protons labeled for reference to signals in the STD spectrum. Peaks with an asterisk are attributed to buffer components. The spectrum was collected at 600 MHz, 25 °C.

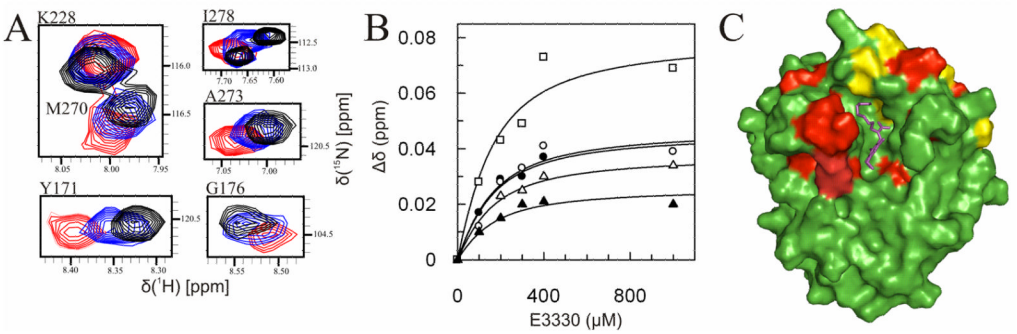

Fig. 5.

E3330 binds to W280A variant of APE1$^{\Delta N38}$. (A) Close-up views of E3330-induced chemical shift changes for some strongly perturbed residues; including spectra for free protein (black) and for E3330:protein ratios of 1:1 (blue) and 10:1 (red). ^{15}N-HSQC spectra were collected at 600 MHz, 25 °C. (B) Binding affinity of APE1$^{\Delta N38}$-W280A for E3330 was determined from the dependence of shift perturbation (Δδ) on E3330 concentration using DynaFit and global fitting, giving K_d = 107 ± 21 μM. Fitting included data for Y171 (□), G176 (○), K228 (▲), M270 (△), and A273 (●). (C) Surface representation of APE1-W280A with E3330 (purple stick) bound as determined by molecular docking. Residues exhibiting Δδ ≥ 0.01 ppm are colored yellow, and those with Δδ ≥ 0.02 ppm are red. The NMR and docking results indicate E3330 binds the same site as observed for native APE1, but the pocket is expanded by removal of the W280 indole side chain, providing additional protein-E3330 interactions. The structure of the APE1-W280A mutant used for docking was generated with COOT (using PDBID: 1BIX).

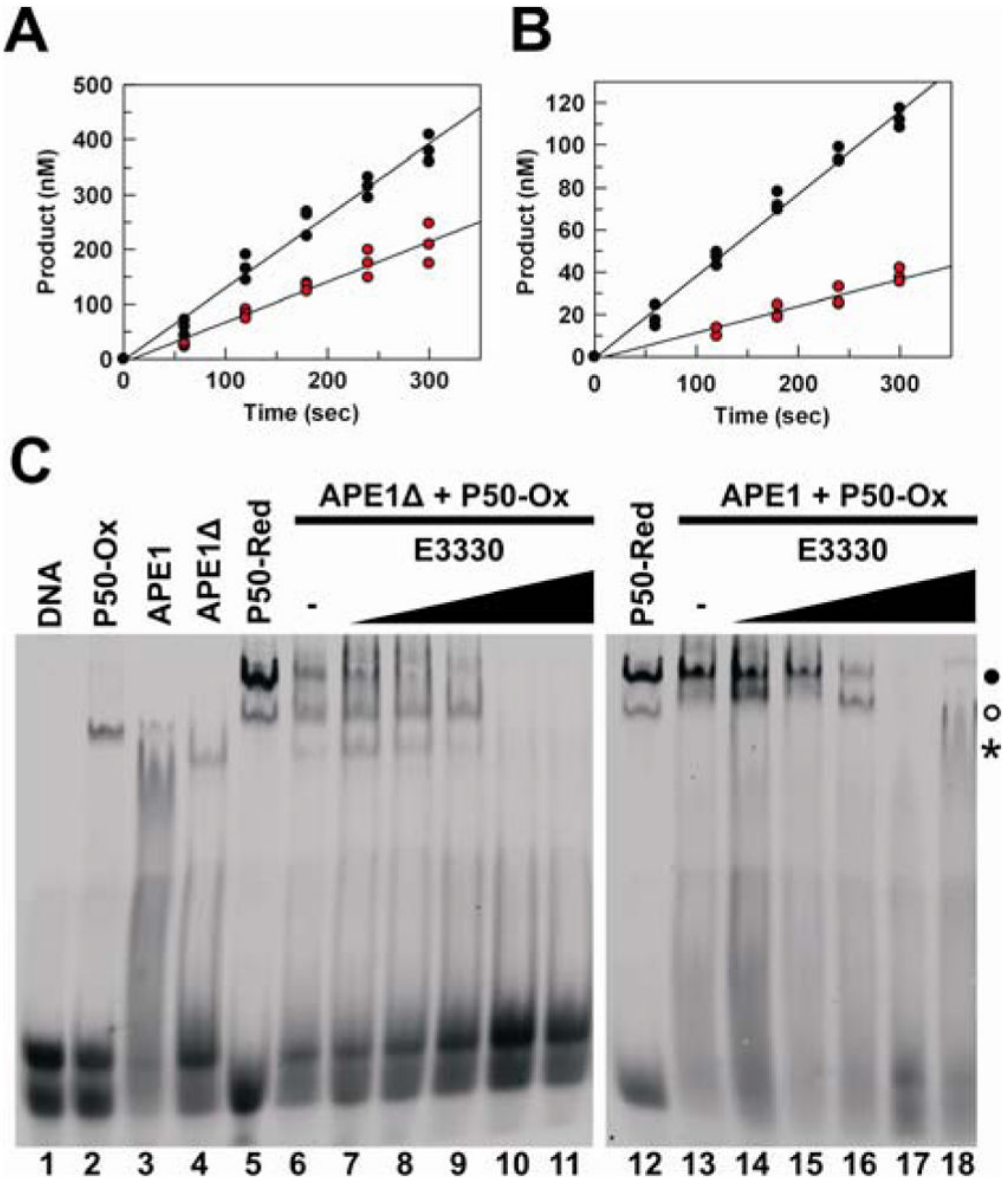

Fig. 6.

E3330 inhibits both repair and redox activity of APE1. Shown are data from steady-state kinetics experiments for (A) $APE1^{\Delta N38}$ (2.5 nM) and (B) full-length APE1 (1 nM) collected with 1 μM AP DNA substrate in the absence (black) or presence (red) of 100 μM E3330. For $APE1^{\Delta N38}$, rate constants are k_{obs} = 0.53 ± 0.02 s^{-1} without E3330 and k_{obs} = 0.29 ± 0.02 s^{-1} with E3330. For APE1, k_{obs} = 0.39 ± 0.01 s^{-1} without E3330 and k_{obs} = 0.13 ± 0.01 s^{-1} with E3330. (C) EMSA results show E3330 inhibits the redox activity of $APE1^{\Delta N38}$ and APE1. Binding of p50 to its cognate DNA (0.1 μM) is much weaker for oxidized p50 (lane 2) relative to reduced p50 (lane 5). DNA binding of oxidized p50 (1.5 μM) is activated by $APE1^{\Delta N38}$ (20 μM, lane 6) and by APE1 (20 μM, lane 13), and activation of p50 by APE1 is inhibited by E3330 (concentrations are 0.2, 0.4, 0.6, 0.8, and 1.0 mM E3330 in lanes 7–11 and 14–18). The protein-DNA bands are annotated as follows: 1:1 p50:DNA, (°); 2:1 p50:DNA, (●); non-specific APE1-DNA binding, (*).

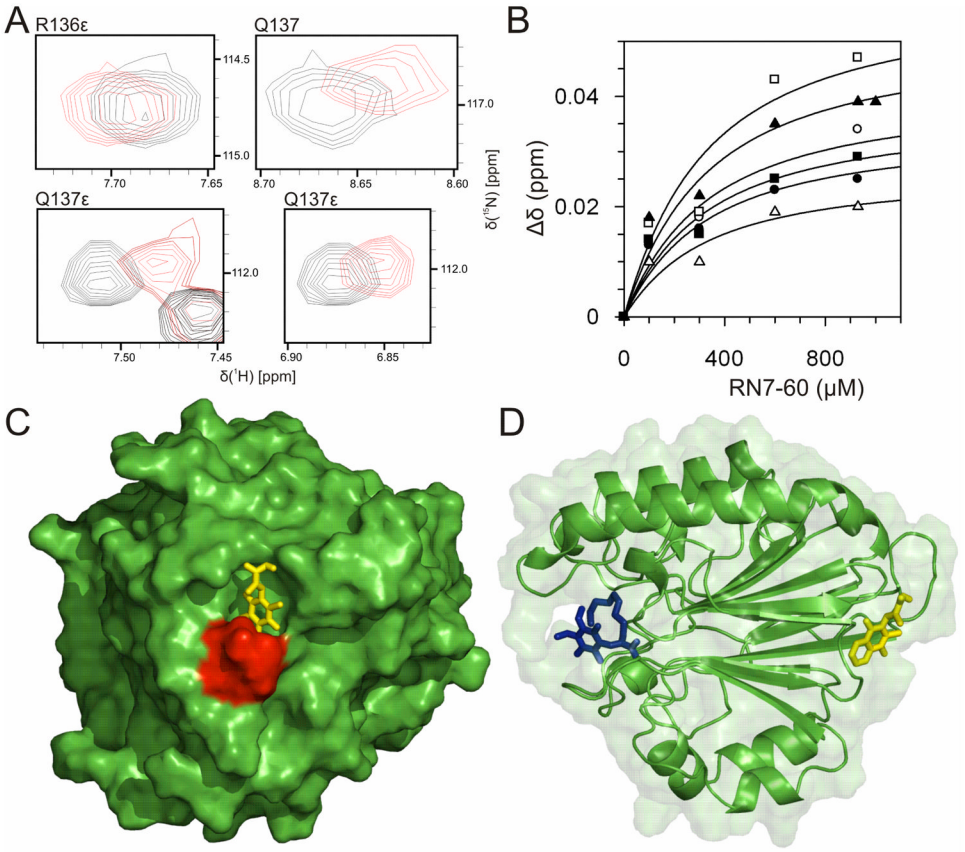

Fig. 7.

Binding of RN7-60 to APE1$^{\Delta N38}$ characterized by NMR and molecular docking studies. (A) Close-up views of shift perturbations induced by RN7-60 for backbone and side-chain N-H resonances of R136 and Q137, including spectra for APE1$^{\Delta N38}$ (100 μM) without ligand (black peaks) and with a 4-fold excess of RN7-60 (red). ^{15}N-HSQC spectra were collected at 600 MHz, 25 °C. (B) The affinity of APE1$^{\Delta N38}$ for RN7-60, K_d = 264 ± 72 μM, was determined from the dependence of shift perturbation (Δδ) on RN7-60 E3330 concentration using DynaFit and global fitting, including data for Q137 (○), Q137 side chain (●), Q137 side chain (□), Q137 side chain (▲), and R136 side chain (△). (C) Surface representation of APE1 with RN7-60 (yellow) bound as determined by molecular docking, consistent with large shift perturbations (Δδ ≥ 0.02 ppm) for R136 and Q137 (colored red). (D) The binding site for RN7-60 (yellow) is on the opposite surface of APE1 relative to the site for E3330 (blue).